The role of temperature and drying cycles on impurity deposition in drying porous media

E. K. LUCKINS[1(a)], C. J. W. BREWARD[2], I. M. GRIFFITHS[2] and C. P. PLEASE[2]

[1] *Mathematics Institute, University of Warwick - Coventry CV4 7AL, UK*
[2] *Mathematical Institute, University of Oxford - Oxford, OX2 6GG, UK*

Abstract – We consider a liquid containing impurities saturating a porous material; when the liquid evaporates, the impurities are deposited within the material. Applications include filtration and waterproof textiles. We present a mathematical model incorporating coupling between evaporation, accumulation and transport of the impurities, and the impact of the deposited impurities on the transport of both the suspended impurities and the liquid vapour. By simulating our model numerically, we investigate the role of temperature and repeated drying cycles on the location of the deposited impurities. Higher temperatures increase the evaporation rate so that impurities are transported further into porous material before depositing than for lower temperatures. We quantify two distinct parameter regimes in which the material clogs: i) the dry-clogging (high-temperature) regime, in which impurities are pushed far into the material before clogging, and ii) the wet-clogging (high-impurity) regime, in which liquid becomes trapped by the clogging. Clogging restricts the extent to which drying time can be reduced by increasing the temperature.

Introduction. – As dirty liquid evaporates from within a porous material, it leaves the impurities that were suspended in the liquid behind. In many practical settings it is important to understand how and where these impurities are deposited within the porous structure. For example, between filter uses, contaminated water remains within the filter and contaminant may be deposited within the filter pores if the water subsequently evaporates [1]. Similarly, impurities accumulate within waterproof membranes (such as raincoats) as they dry after use [2–4]. These processes involve coupled evaporation, transport, and deposition, and related phenomena include the salt weathering of rock [5,6] and the coffee-ring effect [7–9]. Whatever the situation, it is necessary to understand where deposited impurities accumulate within the porous material and, especially, whether the porous material becomes clogged with impurities, as this may impact the efficacy of the filter [10,11], or the hydrophobicity or breathability properties of the waterproof clothing [4]. Wetting and drying cycles are typically repeated many

times in the lifespan of a filter or membrane, and it is unclear how this affects the build-up of deposited impurities [1,11]. Typically, few aspects of the drying process can be controlled except for the temperature, which impacts the drying rate and thus the relative rates of evaporation, transport, and deposition. It is therefore crucial to understand the role that temperature plays in controlling the distribution of deposited impurities, to avoid unwanted impurity deposition profiles or material clogging.

The drying of a wet porous medium and the transport and deposition of impurities are coupled processes. As liquid evaporates, the impurities concentrate, which increases the likelihood of deposition. Furthermore, because this increase in impurity concentration occurs near the liquid surface, it reduces the vaporisation rate of the liquid [12]. The impurities may diffuse within the liquid, but may also be advected by a capillary-driven liquid flow, caused by the evaporation [13]. The transport of liquid, impurities, and vapour are also impacted by the build-up of deposited impurities, which reduce the local porosity. In order to predict the drying behaviour and the resulting deposited impurity profile within the porous material, it is

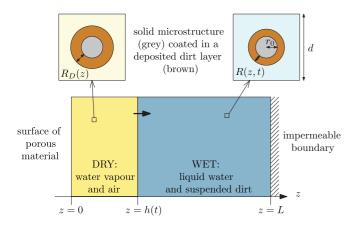(a)E-mail: ellen.luckins@warwick.ac.uk (corresponding author)

Fig. 1: Schematic of a drying porous medium, showing wet and dry regions separated by the moving evaporation front at $z = h(t)$. Insets show the growing layer of deposited dirt, thickness $R(z,t)$, on the porescale structure in the wet region, and the (non-growing) dirt layer, thickness $R_D(z)$ in the dry region.

necessary to understand these coupled processes of evaporation, impurity accumulation, transport, and deposition.

We consider a porous material initially saturated with water containing suspended dirt as the impurity. We present a mathematical model for dirt deposition in porous media that captures many of the coupled effects, but neglect capillary forces and liquid flows. This no-liquid-flow assumption is reasonable for sufficiently deep porous media [13], or for hydrophobic materials that suppress capillary action [14]. Our model is derived by homogenising a porescale model to give a tractable model that holds over the entire porous medium and systematically incorporates the porescale processes [15,16]. Since we neglect liquid flow and capillary effects, there is a sharp drying front between wet and dry regions of the porous medium, and the suspended dirt is only transported through the water by diffusion. We use our model to understand the role of temperature on the deposited dirt profile, and investigate the effect of repeated wetting and drying cycles.

Model statement. – We study a one-dimensional porous material, residing between $z = 0$ (open surface) and $z = L$ (impermeable surface) with two-dimensional, circular (radius r_0) solid inclusions forming the pores (fig. 1). The evaporation front $z = h(t)$ separates a fully dry region (occupied by a mixture of water vapour, density $\rho(z,t)$, and air) from a fully saturated region (occupied by suspended dirt, with volume fraction $\theta(z,t)$ *within the porespace*, and water). The evaporation front $z = h(t)$ moves through the porous material at a speed controlled by the transport of vapour out of the material. The suspended dirt is locally concentrated by the evaporation of water. It diffuses through the wet region, and deposits onto the walls of the microscale pores in a layer of thickness $R(z,t)$, with deposition rate proportional to the local

pore volume fraction θ. The deposited layer of dirt is left behind as the medium dries, and does not evolve while in the dry region, so that the dirt-layer thickness in the dry region, $R_D(z)$, only varies in space. The deposited dirt alters the porosity $\phi(R)$ of the material, with

$$\phi(R) = 1 - \frac{\pi(r_0 + R)^2}{d^2}. \tag{1}$$

As derived in the companion paper [15], our model incorporates evaporation, dirt transport, and deposition. In the dry region, $z \in (0, h(t))$, vapour is transported by diffusion and advection due to the change in density of water as it evaporates, while the deposited dirt-layer thickness R_D does not evolve, so that

$$\phi\frac{\partial\rho}{\partial t} - \phi(R(h(t),t))\left(\frac{\rho_L}{\rho_G} - 1\right)\frac{\partial h}{\partial t}\frac{\partial\rho}{\partial z} = D_v\frac{\partial}{\partial z}\left(\mathcal{D}\frac{\partial\rho}{\partial z}\right), \tag{2a}$$

$$\frac{\partial R_D}{\partial t} = 0. \tag{2b}$$

In the wet region, $z \in (h(t), L)$, suspended dirt diffuses through the water and deposits on the solid microstructure at rate $k\theta$, linear in the volume fraction, θ, of the suspended dirt. This causes the deposited dirt-layer thickness R to increase at the same rate. Thus, in the wet region

$$\phi\frac{\partial\theta}{\partial t} = D_d\frac{\partial}{\partial z}\left(\mathcal{D}\frac{\partial\theta}{\partial z}\right) - \frac{k}{d}\mathcal{C}(\theta_* - \theta)\theta, \tag{2c}$$

$$\frac{\partial R}{\partial t} = k\theta. \tag{2d}$$

The boundary conditions are

$$\rho = 0, \qquad\qquad \text{at } z = 0, \tag{2e}$$

$$\frac{\partial\theta}{\partial z} = 0, \qquad\qquad \text{at } z = L, \tag{2f}$$

$$\rho = \rho_*(T)(1 - \theta), \qquad \text{at } z = h(t), \tag{2g}$$

$$D_v\mathcal{D}\frac{\partial\rho}{\partial z} = \rho_L\left(1 - \frac{\rho}{\rho_G}\right)\phi\frac{\partial h}{\partial t}, \quad \text{at } z = h(t), \tag{2h}$$

$$\phi\theta\frac{\partial h}{\partial t} + D_d\mathcal{D}\frac{\partial\theta}{\partial z} = 0, \qquad \text{at } z = h(t), \tag{2i}$$

assuming that at $z = 0$ the vapour is instantaneously removed (*e.g.*, by a fast flow of air over the surface) and no dirt passes through $z = L$. At $z = h(t)$ we conserve the mass of the volatile component and the suspended dirt, which does not pass through the interface. We also assume that the vapour is in chemical equilibrium with the liquid. This means that ρ takes its saturation value $\rho_*(1 - \theta)$ at $z = h(t)$, which depends on the suspended dirt volume fraction θ. The saturation vapour density of water vapour, ρ_*, is around $2 \times 10^{-2}\,\text{kg m}^{-3}$ (for around $20\,°\text{C}$), but is strongly temperature-dependent [17]. We assume that the system is isothermal, but that the saturation vapour density ρ_* is an increasing function of temperature T. Thus, we write $\rho_*(T)$ in eq. (2g), and view ρ_*

Table 1: Physically relevant parameter values. We assume that the dirt layer is deposited with a volume fraction $\theta_* = 1$, so no water is trapped in the deposited layer. We choose k so that the deposition occurs over a similar timescale to the drying.

Parameter	Description	Value	Reference
d	Interpore spacing	$10^{-6}\,\mathrm{m}$	[18]
r_0	Solid inclusion radius	$0.2d$	–
L	Depth of porous material	$10^{-3}\,\mathrm{m}$	[18]
D_v	Diffusivity of water vapour in air	$2.5 \times 10^{-5}\mathrm{m^2s^{-1}}$	[19]
D_d	Diffusivity of suspended dirt in water	$10^{-9}\mathrm{m^2s^{-1}}$	[19]
ρ_L	Liquid water density	$10^3\mathrm{kgm^{-3}}$	[20]
ρ_G	Air density	$1\mathrm{kgm^{-3}}$	[21]
θ_*	Volume fraction of deposited dirt layer	1	–
k	Dirt deposition rate constant	$5 \times 10^{-9}\mathrm{ms^{-1}}$	–
ρ_*	Vapour saturation density	$2 \times 10^{-2}\mathrm{kgm^{-3}}$	[17]

as a proxy for T. While other system parameters, namely D_v, D_d and k may also exhibit temperature variations, we estimate that these are less pronounced than for ρ_*, which undergoes an order of magnitude change over the range 10–60 °C. Thus, we neglect any other temperature dependence in the system. Initially (at $t = 0$), we assume

$$H = 0, \qquad R = 0, \qquad \theta = \theta_I, \tag{2j}$$

with θ_I uniform. Like the porosity ϕ, given by (1), the effective diffusivity $\mathcal{D}$ (capturing the effect of the pore-structure on diffusivity), and surface area of the deposited dirt layer $\mathcal{C}$ are dimensionless functions of R or R_D (in the wet and dry regions, respectively), with

$$\mathcal{C} = \frac{2\pi(r_0 + R(z,t))}{d}, \tag{3}$$

and $\mathcal{D}$ given by the solution of a cell problem [22,23], which varies monotonically from $\mathcal{D} = 1$ when $R = 0$ to $\mathcal{D} = 0$ when $R = R_\text{clog} = d/2 - r_0$. The porosity, ϕ, and effective diffusivity, $\mathcal{D}$, of the medium depend on R and, therefore, the transport of both the suspended dirt and the water vapour depend on where the dirt has previously deposited. The model parameters are listed in table 1 along with approximate values that we will use in our numerical simulations.

Drying behaviour and the effect of temperature on drying. – In our model (2), vapour is transported from the evaporation front to the surface by both diffusion and advection, with the flow being generated by the change in density of the water as it vaporises. The timescale for drying is estimated from a balance in eq. (2h), giving

$$\text{drying timescale} = \frac{L^2 \rho_L}{D_v \rho_*} \approx 33\,\text{minutes.} \tag{4}$$

We numerically simulate (2) using the method of lines with central differences for diffusive terms, and up-winding for advection. At a given temperature, the evaporation front moves fastest initially and then slows over time as the evaporation front moves further into the porous material, reducing the vapour density gradient and hence the vapour flux (fig. 2(a)). Suspended dirt is concentrated by removal of water by evaporation, accumulating near $z = h(t)$, so the volume fraction $\theta(z,t)$ of suspended dirt is largest at $z = h(t)$ (fig. 2(b)). Dirt deposits on the microstructure at a rate proportional to the local suspended dirt volume fraction, and, therefore, deposition is fastest at the evaporation front. This, along with the temporal variation in the evaporation front speed, leads to an internal peak in the final deposited dirt thickness $R_D(z)$ (fig. 2(c)).

Higher temperatures correspond to higher values of ρ_*, thus faster evaporation, since there is a steeper gradient in ρ (fig. 2(b)). In turn, faster motion of the evaporation front leads to faster accumulation of suspended dirt relative to its deposition, seen in the increased θ-values (fig. 2(b)) (which are at the same stage $h = 0.2L$ in the drying). Therefore, for higher temperatures we observe (fig. 2(c)) that suspended dirt is pushed further into the porous medium before it deposits.
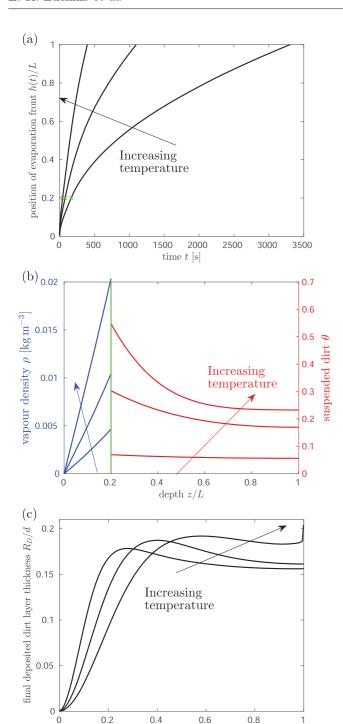
Fig. 2: The role of temperature on drying dynamics and resultant deposited dirt profile. Solutions for three temperatures, corresponding to $\rho_* = (0.5, 1.5, 4.5) \times 10^{-2} \, \text{kg m}^{-3}$, are shown, and we take $\theta_I = 0.3$. (a) The position $h(t)$ of the evaporation front against time. (b) The vapour density profile ρ and suspended dirt volume fraction θ in the material, at the times shown by green crosses in (a). (c) The final deposited dirt-layer profile $R_D(z)$ once the drying is complete. Larger ρ_* corresponding to higher temperatures result in a higher and wider peak in the deposited dirt-layer profile, further from the surface of the porous material, since evaporation at higher temperatures is faster relative to the dirt deposition, and so dirt is pushed further into the material before depositing.

Clogging behaviours. – The spatially non-uniform deposited dirt layer may lead to clogging of the porous material in certain parameter regimes. The system is said to have clogged if, at a particular time, the dirt-layer thickness R reaches its maximum possible value, R_{clog}, so that —in our simple two-dimensional microscale geometry— the neighbouring circles of deposited dirt meet, and the effective diffusivity $\mathcal{D}(R_{\text{clog}}) = 0$. When the material clogs, evaporation ceases, since the vapour cannot be transported past the point where $\mathcal{D} = 0$. Since deposition occurs fastest at the moving interface $z = h(t)$, this is where clogging happens (if it occurs). Clogging is not specific to our choice of microscale geometry: for any given pore geometry there is a maximum dirt-layer thickness at which the porespace ceases to be a connected domain.

There are two distinct clogging mechanisms inherent to the model (2):

1) *Wet-clogging* (fig. 3(a)) when $R = R_{\text{clog}}$ while h is small, where water is trapped within the pore-structure behind the clog point. Wet-clogging only occurs for sufficiently high initial volume fractions, θ_I, of the dirt, and for sufficiently fast dirt deposition relative to evaporation.

2) *Dry-clogging* (fig. 3(b)) occurs when the rate of dirt deposition is sufficiently slow relative to evaporation, so that suspended dirt is pushed ahead of the evaporation front, accumulating until θ is close to 1. As $\theta \to 1$, the evaporation slows considerably (if there were no dirt deposition, the system would approach $\theta = 1$ in infinite time [15]). Since the evaporation is slow, deposition becomes significant, and R grows to R_{clog}. A negligible volume of water is trapped by dry-clogging in $z > h(t)$, since θ is close to 1. (The highest temperature situation shown in fig. 2 operates very close to the dry-clogging limit, since we see in fig. 2(c) that there is a very rapid increase in R_D near to $z = L$.)

In practical applications, it may be important to dry material quickly, which is achievable by increasing the temperature, but it is important to avoid clogging in order to maintain filter functionality or the breathability of waterproof clothing. We quantify the parameter regimes for which the material clogs by considering the final position, h_{end}, of the evaporation front (*i.e.*, its position when the evaporation ceases) as a function of both the initial dirt volume fraction θ_I and the saturation vapour density ρ_* (which we assume monotonically increases with temperature) (fig. 4(a)). If the evaporation front reaches the end of the domain, $h_{\text{end}} = L$ and there is no clogging. We observe that $h_{\text{end}} = L$ if both the initial dirt volume fraction θ_I is sufficiently small, and ρ_* (or temperature) is sufficiently low. There is a critical initial dirt volume fraction, θ_I^*, around 0.6 above which we see wet-clogging, with h_{end} significantly below L. We see that θ_I^* is largely
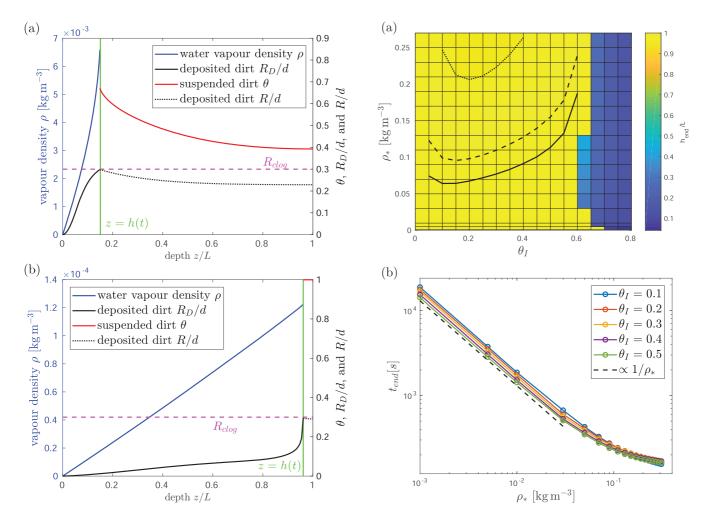
Fig. 3: Two distinct clogging mechanisms inherent to (2). (a) *Wet-clogging*, with $\theta_I = 0.7$, $\rho_* = 0.02\,\text{kg m}^{-3}$, where the deposited dirt-layer thickness reaches its maximum $R_{\text{clog}} = 0.3$ while the suspended dirt volume fraction $\theta < 1$ and water is trapped within the material when evaporation ceases. (b) *Dry-clogging*, with $\theta_I = 0.1$, $\rho_* = 0.2\,\text{kg m}^{-3}$, where dirt deposition is slow relative to evaporation, and accumulation results in $\theta \approx 1$ as the system clogs.

Fig. 4: The effect of temperature and initial dirt level on clogging and drying time. (a) Colour shows the final position of the evaporation front h_{end}, varying the initial suspended dirt volume fraction, θ_I, and the saturation vapour density, $\rho_*(T)$. We see wet-clogging above a critical θ_I, which is largely independent of ρ_*. Dry-clogging is observed as ρ_* is increased: the black lines are the curves $h_{\text{end}}/L = 0.99$ (solid line), 0.98 (dashed line), and 0.95 (dotted line). (b) End time t_{end} as a function of the saturation vapour density ρ_* for various θ_I (chosen so there is no wet-clogging). The drying time is inversely proportional to the saturation density at low ρ_*, but drying is limited by suspended dirt diffusion at higher temperatures (higher ρ_*).

independent of temperature for most values of ρ_* (or temperature). However, at very low temperatures, we are able to dry fully with slightly higher dirt loads without wet-clogging. This is because, by drying slowly at low temperature, the dirt deposition is spatially uniform to a first approximation, only minimally affected by suspended dirt accumulation at the evaporation front. An upper bound on θ_I^* is estimated by supposing dirt deposition is uniform (the limit of infinitely slow evaporation), giving

$$\theta_I^* < 1 - \frac{\phi(R_{\text{clog}})}{\phi(0)} = 0.755 \tag{5}$$

for the parameter values used in fig. 4. In practice, we see that wet-clogging occurs for θ_I below this upper bound due to the non-uniform dirt deposition profile due to evaporation.

For $\theta_I < \theta_I^*(\rho_*)$, h_{end} is close to L. However, at larger ρ_* we see h_{end} decrease below L as dry-clogging begins: the solid, dashed and dotted black contours show where h_{end} is 1%, 2% and 5%, respectively, away from the end of the domain. Generally, at higher temperatures (greater ρ_*), deposition is slower relative to evaporation, pushing the system towards dry-clogging. These contours are not horizontal due to the dependence of the deposition and evaporation rates (via eq. (2g)) on θ: for a fixed temperature (or ρ_*) the dirt deposition rate is proportional to θ. Thus for smaller θ_I (with slower deposition rate) dry-clogging is less prominent. Meanwhile, for large θ,
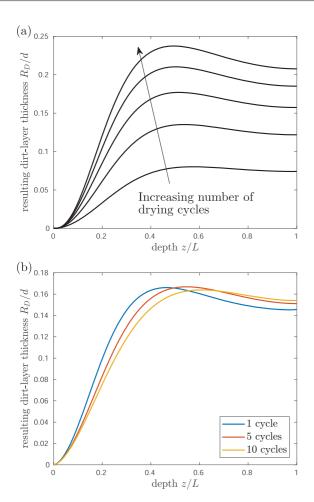
Fig. 5: Multiple repeated wetting and drying cycles. (a) Resulting dirt deposition profiles after each of five successive drying cycles, with the same initial dirt level $\theta_I = 0.1$ for each cycle. The arrow moves from the first drying cycle to the last. (b) Resultant dirt deposition profiles for different numbers of repeated drying cycles: here the same total amount of dirt is deposited, but over a different number of drying cycles.

evaporation is slowed due to suspended dirt accumulation at $z = h$, again reducing the dry-clogging effect.

The time t_{end} at which drying completes (*i.e.*, h reaches h_{end}) also depends on both temperature (via ρ_*) and θ_I (fig. 4(b)). Here we consider only $\theta_I < \theta_I^*$ so that there is no wet-clogging. At low temperatures (small ρ_*) the drying time is seen to be inversely proportional to ρ_*. However, as the temperature or ρ_* increases, we see that the drying time does not continue to decrease. Instead, the evaporation becomes limited by the diffusive transport of suspended dirt away from the evaporation front, which occurs over a timescale of around $L^2/D_d \approx 10^3$ s. The dependence of the drying time on θ_I is relatively small: we observe faster drying at higher dirt volume fractions since there is less water in the system to evaporate.

Overall, to minimise drying time we have seen that we should dry at higher temperatures. However, beyond a certain point the drying rate is limited by suspended dirt

diffusion away from the evaporating interface and so increasingly higher temperatures yield limiting returns. Furthermore, at higher temperatures dry-clogging begins to take effect, creating a region of blocked filter that compromises its future functionality.

Multiple drying cycles. – We also investigate the effect of multiple repeated wetting and drying cycles. Starting with $R = 0$ everywhere, we simulate drying a material, initially saturated with a $\theta_I = 0.1$ dirt solution, until $h = L$ (no clogging occurs for these parameter values). We then take the final deposited dirt profile $R_D(z)$ and restart the model with this as the initial deposited dirt profile, and with $\theta_I = 0.1$ again, and repeat for many cycles. The internal peak in $R_D(z)$ is accentuated with each repeated cycle (fig. 5(a)). This is because the local porosity ϕ and effective diffusivity $\mathcal{D}$ depend on the previous cycles' dirt deposition. (Subsequent additional wetting and drying cycles would eventually lead to wet-clogging.)

We also compare the resulting deposited dirt profiles when the same total amount of dirt, $\theta_{TOT}\phi(0)L$ per unit cross-sectional area, has been deposited, but over a different number of these repeated wetting/drying cycles (fig. 5(b)): at the start of each drying cycle we impose $\theta_I = 1 - (1 - \theta_{TOT})^{1/N}$, where N is the number of drying cycles ($N = 1, 5$, and 10 in fig. 5(b)). The more cycles we take to deposit the dirt, the further into the porous material the dirt is pushed before depositing, with a peak R_D deeper into the porous material (fig. 5(b)). This is because, since the deposition rate is proportional to θ, for larger N (more cycles) θ is smaller and, therefore, the deposition rate is slower during each cycle, while the evaporation rate remains roughly the same for different N. This suggests that clogging due to accumulation over many cycles is likely to occur deeper within the porous material than over a single cycle.

Conclusion. – Our model captures the nonlinear coupled relationships between evaporation, vapour transport, dirt accumulation, transport, and deposition, as a dirt–water mixture is dried in a porous material. Both the drying dynamics and resulting distribution of deposited dirt through the porous material are seen to depend on the temperature of the drying. Furthermore, we identify parameter regimes in which the porous medium clogs. In particular, we see that higher temperatures result (as expected) in faster drying, albeit with limited returns, as at sufficiently high temperatures the drying becomes limited by the transport of suspended dirt away from the evaporation front. Furthermore, too high a temperature results in the dry-clogging of the material, by which the porespace at the end of the medium is fully clogged with dirt. The fastest drying that can be achieved is therefore at the highest temperature for which dry-clogging does not occur. These results are expected to be valuable in the filtration and waterproof textiles industries for optimisation of filter membrane cleaning and

drying procedures in order to maximise filter lifespan and functionality.

REFERENCES

[1] Ji H. and Sanaei P., *Phys. Rev. Fluids*, **8** (2023) 064302.
[2] Breward C. J. W., Brosa Planella F., Edwards D. A., Kiradjiev K., Kovacs A., Llewellyn Smith S., Rumschitzki D., Sanaei P., Sun Y., Witelski T., Zyskin M., Tilley B., Broadbridge P., Gu B., Adriazola J., Barra V., Fok P.-W., Ockendon H. and Ockendon J., *Evaporation from porous media, pore-level analysis*, 36th MPI Workshop report, University of Vermont, `https://mpi2020.w3.uvm.edu/finalReports/FinalReport_Gore_2020.pdf` (2020).
[3] Sanaei P., Breward C. J. W., Ellis M. A., Han S., Holzer B., Ji H., El Kahza H., Llewellyn Smith S. G., Parsa S., Reynolds H., Troy J., Witelski T., Zhang N. and Zyskin M., *Mathematics in Industry Reports*, Cambridge Open Engage, doi:10.33774/miir-2022-wq8fl.
[4] Tehrani-Bagha A. R., *Adv. Colloid Interface Sci.*, **268** (2019) 114.
[5] Oguchi C. T. and Yu S., *Prog. Earth Planet. Sci.*, **8** (2021) 1.
[6] Rodriguez-Navarro C. and Doehne E., *Earth Surf. Processes Landforms: J. Br. Geomorphol. Res. Group*, **24** (1999) 191.
[7] Mampallil D. and Eral H. B., *Adv. Colloid Interface Sci.*, **252** (2018) 38.
[8] Moore M. R., Vella D. and Oliver J. M., *J. Fluid Mech.*, **920** (2021) A54.
[9] Soltman D. and Subramanian V., *Langmuir*, **24** (2008) 2224.
[10] Agranovski I. E. and Shapiro M., *Chem. Eng. Technol.: Industrial Chem-Plant Equipment-Process Eng.-Biotechnol.*, **24** (2001) 387.
[11] Yong C. F., Deletic A., Fletcher T. D. and Grace M. R., *The drying and wetting effects on clogging and pollutant removal through porous pavements*, in *Proceedings of the 7th International Conference on Sustainable Techniques and Strategies for Urban Water Management* (GRAIE, Lyon, France) 2010, pp. 1–10.
[12] Karapetsas G., Sahu K. C. and Matar O. K., *Langmuir*, **32** (2016) 6871.
[13] Lehmann P., Assouline S. and Or D., *Phys. Rev. E*, **77** (2008) 056309.
[14] Shokri N., Lehmann P. and Or D., *Geophys. Res. Lett.*, **35** (2008) L19407.
[15] Luckins E. K., Breward C. J. W., Griffiths I. M. and Please C. P., to be published in *J. Fluid Mech.* (2024).
[16] Luckins E. K., Breward C. J. W., Griffiths I. M. and Please C. P., *Eur. J. App. Math.*, **34** (2023) 806.
[17] Wexler A., *J. Res. Nat. Bureau Standards. Sect. A, Phys. Chem.*, **80** (1976) 775.
[18] Feng S., Zhong Z., Wang Y., Xing W. and Drioli E., *J. Membrane Sci.*, **549** (2018) 332.
[19] Cussler E. L., *Diffusion: Mass Transfer in Fluid Systems*, 3rd edition (Cambridge University Press, Cambridge, UK) 2009.
[20] Bigg P. H., *Br. J. Appl. Phys.*, **18** (1967) 521.
[21] Tsilingiris P. T., *Energy Conversion Manag.*, **49** (2008) 1098.
[22] Bruna M. and Chapman S. J., *SIAM J. Appl. Math.*, **75** (2015) 1648.
[23] Dalwadi M. P., Griffiths I. M. and Bruna M., *Proc. R. Soc. A: Math. Phys. Eng. Sci.*, **471** (2015) 20150464.